Effects of NaCl Concentration and Solution Temperature on the Galvanic Corrosion between CFRP and AA7075T6

S. Y. Hur, K. T. Kim, Y. R. Yoo, and Y. S. Kim†

Materials Research Centre for Energy and Clean Technology,
School of Materials Science and Engineering, Andong National University,
1375 Gyeongdong-ro, Andong, Gyeongbuk, 36729, Korea

To reduce structural weight, light metals, including aluminum and magnesium alloys, have been widely used in various industries such as aircraft, transportation and automobiles. Recently, composite materials such as Carbon Fiber Reinforced Plastics (CFRP) and Graphite Epoxy Composite Material (GECM) have also been applied. However, aluminum and its alloys suffer corrosion from various factors, which include aggressive ions, pH, solution temperature and galvanic contact by potential difference. Moreover, carbon fiber in CFRP and GECM is a very efficient cathode, and very noble in the galvanic series. Galvanic contact between carbon fiber composites and metals in electrolytes such as rain or seawater, is highly undesirable. Notwithstanding the potentially dangerous effects of chloride and temperature, there is little research on galvanic corrosion according to chloride concentration and temperature. This work focused on the effects of chloride concentration and solution temperature on AA7075T6. The increased galvanic corrosion between CRFP and AA7075T6 was evaluated by electrochemical experiments, and these effects were elucidated.

Keywords: CFRP, AA7075, Galvanic Corrosion, NaCl Concentration, Solution Temperature

1. Introduction

Aluminum and its alloys suffer corrosion from various factors, which include aggressive ions, pH, and solution temperature [1,2]. Among these factors, chloride ion can be adsorbed on the surface faster than other species and deteriorate the passive film at lesser potential than pitting potential, and when its concentration increased, the current density and corrosion rate increase [3,4]. A high chloride concentration supports a fast initiation rate, but it will also accelerate the protective precipitation of corrosion product. Low chloride concentration leads to slower initiation, but also a slower precipitation process, leading to more uniform corrosion in the long term [5]. When exposed to environments containing halide ions, of which the chloride (Cl^-) ion is the most frequently encountered in service, the oxide film breaks down at specific points leading to the formation of pits on the aluminum surface [6]. At higher temperatures, the pitting potential decreases with increasing temperature and chloride concentration [7].

Therefore, as the temperature increases, the pitting potential decreases, resulting in pitting corrosion rather than uniform corrosion.

Non-metallic composite materials, for example, GECM show high specific strength, because of their low density. These kinds of non-metallic composite material improve the structural effectiveness and operation economics. However, if these materials contact several metals, corrosion can arise, since non-metallic materials have electrical conductivity [8]. Galvanic coupling between GECM and metallic materials can facilitate the corrosion of metals and alloys because GECM is noble and electrically conductive. Galvanic corrosion can be affected by many factors including metallic materials, area ratio, surface condition, and corrosivity. In the case of galvanic coupling of carbon steel and aluminum to GECM, corrosion rate increased with increasing area ratio [9]. Galvanic corrosion of metallic materials by GECM was improved when metallic materials were treated using electrochemical anodizing and thermal oxidation [10].

It should be noted that carbon fiber is a very efficient cathode and very noble in the galvanic series. Galvanic contact between carbon fiber composites and metals in electrolytes such as rain or seawater is highly undesirable.

---

†Corresponding author: yikim@anu.ac.kr
S. Y. Hur: Master, K. T. Kim: Postdocs, Y. R. Yoo: Research Professor,
Y. S. Kim: Professor

If galvanic coupling forms, galvanic corrosion of the metal may occur. [11]. Specifically, the CFRP/Al sheets and CFRP sheet/Al rivet were formed for electrochemical couple respectively, so as to activate the galvanic corrosion phenomenon [12]. CFRP acted as cathode, while Al acted as anode. Thus, the Al sheet would induce anodic dissolution. It is well known that CFRP and aluminum can form a strong galvanic couple, resulting in severely accelerated corrosion of the aluminum, particularly if the electrolyte contains chloride ions. In chloride containing-solutions, they tend towards pitting corrosion, which can endanger the structural integrity [13,14]. The recent demand for better fuel-efficiency in the aircraft industry has reflected the increased usage of more lightweight materials such as CFRP and titanium, as well as aluminum [15,16].

The increased application of these "mixed materials" enhances the risk of galvanic corrosion when they are coupled in the presence of a corrosive electrolyte. Since carbon fibers are electrically conductive, the aluminum alloy - carbon system has a tendency to form a galvanic cell, and corrosion of the connecting metal components may occur at an enhanced rate. In particular, graphite, a major component of CFRP, in the previous work [17] revealed the effects of NaCl concentration (0.01 ~ 1% NaCl) and solution temperature (30 ~ 75 $^\circ$C) on the galvanic corrosion between CFRP and A516Gr.55 carbon steel, and the following can be concluded: Since CFRP showed water absorption and high open circuit potential, most metallic materials may be galvanically corroded if the materials make contact with CFRP. The average corrosion rate of single carbon steel increased 0.63% per 10 times concentration, but its rate of steel coupled with CFRP increased 46.9% per 10 times concentration. However, when the temperature increased by 10 $^\circ$C, corrosion rates of single specimen or coupled specimen with CFRP revealed a similar effect, even though the rate of coupled specimen was higher than that of single specimen.

The combination of CFRP and AA7075T6 can be used to reduce the weight of the shaft of some crane structure. Therefore, this work focused on the effect of NaCl concentration and solution temperature on the corrosion between CFRP and AA7075T6 aluminum alloy.

2. Experimental methods

2.1 Materials

Commercial CFRP and aluminum alloy (AA7075 T6) were used in this work. The chemical composition of AA7075 used in the experiments was Al-0.095Si -0.137Fe-1.540Cu-0.008Mn-2.590Mg-0.209Cr-5.590Zn-0

.020Ti [18].

2.2 Polarization test

Specimens were cut to a size of 1.5 mm × 1.5 mm and the surface was ground using #600 SiC paper. The specimen was electrically connected with a rubber-coated Cu wire, and the surface of the specimen was coated with epoxy resin, except for an area of 1 cm^2. Polarization tests were performed using a potentiostat (Gamry Co. Interface 1000, DC105). The reference electrode was a saturated calomel electrode (SCE), and the counter electrode was high-density graphite rods. The test solution was deaerated using nitrogen gas at the rate of 200 mL/min for 30 min and the scanning rate was 0.33 mV/s. NaCl concentration was controlled as (0.01, 0.1, and 1)% NaCl and solution temperature was maintained as (30, 50, and 75) $^\circ$C. Whether crevice corrosion or not after the polarization test was confirmed using a microscopic observation.

2.3 Immersion corrosion test

AA7075T6 specimen was cut to a size of 15 mm × 20 mm × 1.5 mm and each surface was ground using #120 SiC paper. Every specimen was weighed and immersion test was performed for 10 days. Test solution was non-deaerated and after the test, corrosion rate was calculated and the surface appearance was observed by optical microscopy (OM, Axiotech 100HD, Carl Zeiss, Germany).

2.4 Galvanic corrosion test

Specimens were cut to a size of 1.5 mm × 1.5 mm and the surface was ground using #600 SiC paper. The specimen was electrically connected with a rubber-coated Cu wire, and the surface of the specimen was coated with epoxy resin, except for an area of 1 cm^2 . Galvanic corrosion current and potential were measured over 5 hours using a potentiostat (Gamry Co. Interface 1000, DC105). The reference electrode was a saturated calomel electrode (SCE), the working electrode was AA7075 and the counter electrode was CFRP. The distance between the working electrode and the counter electrode was 4cm. Test solutions were non-deaerated 0.1 % NaCl at (30, 50, and 75) $^\circ$C, and (0.01, 0.1, and 1) % NaCl at 50 $^\circ$C. Corrosion rate was calculated using a current-time graph. The surface appearance was observed using optical microscopy (OM, Axiotech 100HD, Carl Zeiss, Germany).

2.5 Pit density measurement

Pit density was obtained at x100 magnification for the tested specimen. The number of pit was counted and then the pit density was calculated as pits per mm^2. Measurement by a total of 3 times gave the average value.

3. Results and discussion

3.1 Effect of NaCl concentration on the galvanic corrosion between CFRP and AA7075T6

Fig. 1 shows the effect of NaCl concentration on the corrosion rate of AA7075T6 by galvanic coupled CFRP. Solution temperature was 50 $^{\circ}$C and non-deaerated x% NaCl
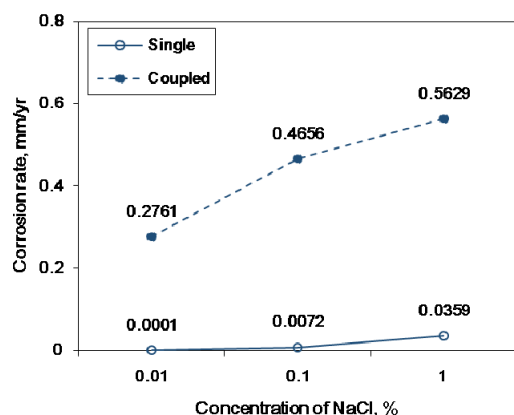
Fig. 1 Effect of NaCl concentration on the corrosion rate of AA7075T6 by galvanic coupled CFRP (Solution temperature: 50 $^{\circ}$C, non-deaerated x% NaCl solution).

solutions were used. In the single AA7075T6 specimen, the corrosion rate increased slightly with increasing NaCl concentration. However, when AA7075T6 was galvanically coupled with CFRP, the corrosion rate of AA7075T6 was drastically increased; at 0.01% NaCl solution, corrosion rate was increased 276,000% by the galvanic effect with CFRP; and at (0.1 and 1)% NaCl solutions, corrosion rates were increased by 6,367% and 1,468 %, respectively, and thus the average galvanic corrosion rate of AA7075T6 by CFRP increased several hundred times over that of the single specimens. On the other hand, for the effect of NaCl concentration, in the case of single specimen, the trend equation (Coefficient of determination, R^2=0.89) between the concentration and corrosion rate was derived as

- 'Corrosion rate = 0.0078 ln [x% NaCl] + 0.0323';
and in the case of galvanic coupled specimen, the trend line (R^2=0.97) was calculated as;

- 'Corrosion rate = 0.0623 ln [x% NaCl] + 0.5783'
from Fig. 1. The relationship between corrosion rate and NaCl concentration reveals a logarithmic trend. It should be noted that the effect of NaCl concentration in the galvanic coupled specimen was *ca.* 8 times higher than that in the single specimen.

Fig. 2 shows the effect of NaCl concentration on the
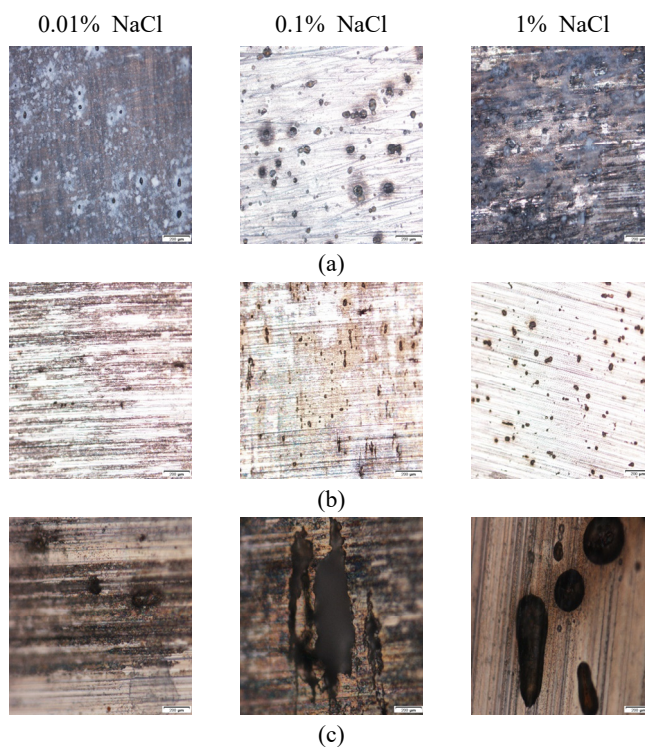
Fig. 2 Effect of NaCl concentration on the surface appearance of AA7075T6 after the corrosion tests (Solution temperature; 50 $^{\circ}$C); (a) single specimen (OM, x100) and (b) galvanic coupled specimen with CFRP (OM, x100) (c) galvanic coupled specimen with CFRP (OM, x1000).
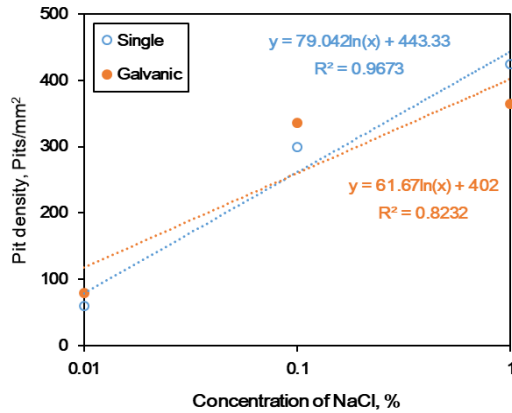
Fig. 3 Relationship between NaCl concentration and pit density of AA7075T6 by galvanic coupling with CFRP (Solution temperature; 50 °C).
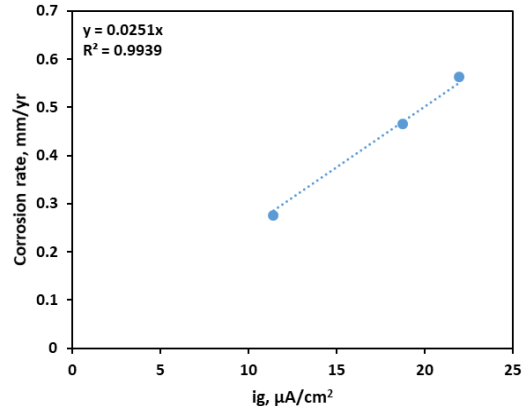
Fig. 5 Effect of NaCl concentration on the relationship between galvanic current density derived from the mixed potential theory using polarization curves and the corrosion rate of AA7075T6 by galvanic coupled CFRP.
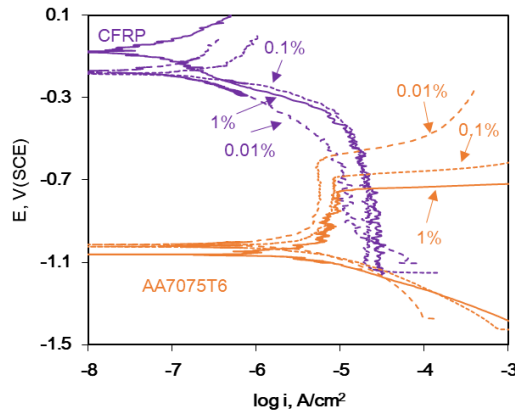
Fig. 4 Overlapped polarization curves of CFRP and AA7075T6 obtained in deaerated (0.01, 0.1, and 1)% NaCl at 50 °C.

surface appearance of AA7075T6 after the corrosion tests. Solution temperature was 50 °C. Fig. 2a shows the single AA7075T6 specimen (OM, x100) and as the concentration increases, the numbers of pits increased, but the shape of pits was almost spherical. Fig. 2b is for the galvanic coupled AA7075T6 specimen with CFRP (OM, x100) and the shape of pits was changed while Fig. 2c confirms that the pits in AA7075T6 specimen were changed from spherical to elongated by the galvanic coupled effect with CFRP (OM, x1000). It is considered that the change of corroded shape can arise because the galvanic effect by CFRP greatly facilitates the corrosion of AA7075T6. Pit density can be calculated from Fig. 2. Fig. 3 shows the relationship between NaCl concentration and pit density of AA7075T6 by galvanic coupling with CFRP. The solution temperature was 50 °C. As the NaCl concentration increases, the pit density was greatly increased, and the relationship

between NaCl concentration and pit density revealed the logarithmic relation trend.

Fig. 4 shows the overlapped polarization curves of CFRP and AA7075T6 obtained in deaerated x% NaCl at 50 °C. Regardless of NaCl solutions, the cathodic polarization curves of CFRP meet the anodic polarization curves above the pitting potentials. This means that galvanic coupling with CFRP can facilitate the corrosion of AA7075T6.

Galvanic corrosion current density can be calculated from Fig. 4 based on the mixed potential theory [19]. Fig. 5 reveals the effect of NaCl concentration on the relationship between galvanic current density (i_g) derived from the mixed potential theory using polarization curves and the corrosion rate of AA7075T6 by galvanic coupled CFRP. Two factors shows the exponential relation:

Corrosion rate, mm/yr = 0.0251 x [i_g, µA/cm^2].

3.2 Effect of solution temperature on the galvanic corrosion between CFRP and AA7075

Fig. 6 depicts the effect of solution temperature on the corrosion rate of AA7075T6 by galvanic coupled CFRP in non-deaerated 0.1% NaCl solution. In the single AA7075T6 specimen, the corrosion rate increased slightly with increasing solution temperature. However, when AA7075T6 was galvanically coupled with CFRP, the corrosion rate of AA7075T6 was drastically increased; at 30 °C, 212,400% of corrosion rate was increased by the galvanic effect with CFRP, and at (50 and 75) °C, corrosion rates were increased by 6,367% and 1,069 %, respectively, and thus the average galvanic corrosion rate of AA7075T6 by CFRP increased several hundred times over that of the single specimens. On the other hand, as for the effect of

solution temperature, in the case of single specimen, the trend equation (Coefficient of determination, R^2=0.89) between the concentration and corrosion rate was derived as:

- 'Corrosion rate = 0.0012x[T, ℃] + 0.042',

and in the case of galvanic coupled specimen, the trend line (R^2=0.96) was calculated as:

- 'Corrosion rate = 0.0089x[T, ℃] + 0.029
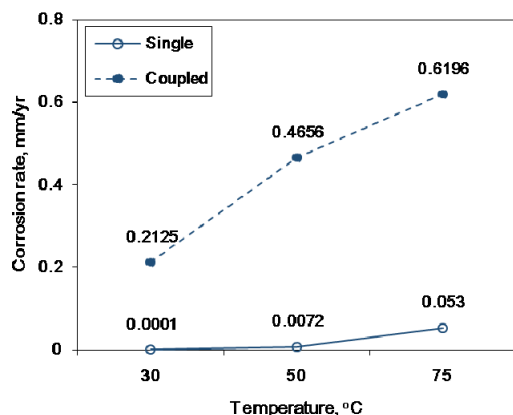
Fig. 6 Effect of solution temperature on the corrosion rate of AA7075T6 by galvanic coupled CFRP in 0.1% NaCl solution.

from Fig. 6. The relationship between corrosion rate and solution temperature reveals a linear trend. It should be noted that the effect of solution temperature in the galvanic coupled specimen was *ca.* 7.4 times higher than that in the single specimen. Since the galvanic potential difference between CFRP and AA7075T6 including chloride ion activity and diffusion rate were increased by increasing the solution temperature, it is considered that galvanic corrosion can be facilitated by increasing the solution temperature.

Fig. 7 shows the effect of solution temperature on the surface appearance of AA7075T6 after the corrosion tests. The solution was 0.1% NaCl. Fig. 7a is for the single AA7075T6 specimen (OM, x100) and as the temperature increases, the numbers of pits was slightly increased but the shape of pits was almost spherical, except at 75 ℃. Fig. 7b shows the galvanic coupled AA7075T6 specimen with CFRP (OM, x100) the shape of pits was changed, and Fig. 7c confirms that the pits in AA7075T6 specimen were changed from spherical to elongated by the galvanic coupled effect with CFRP (OM, x1000). The effect of solution temperature on pit shape was similar to that of NaCl concentration. Fig. 8 reveals the relationship between solution temperature and pit density of AA7075T6
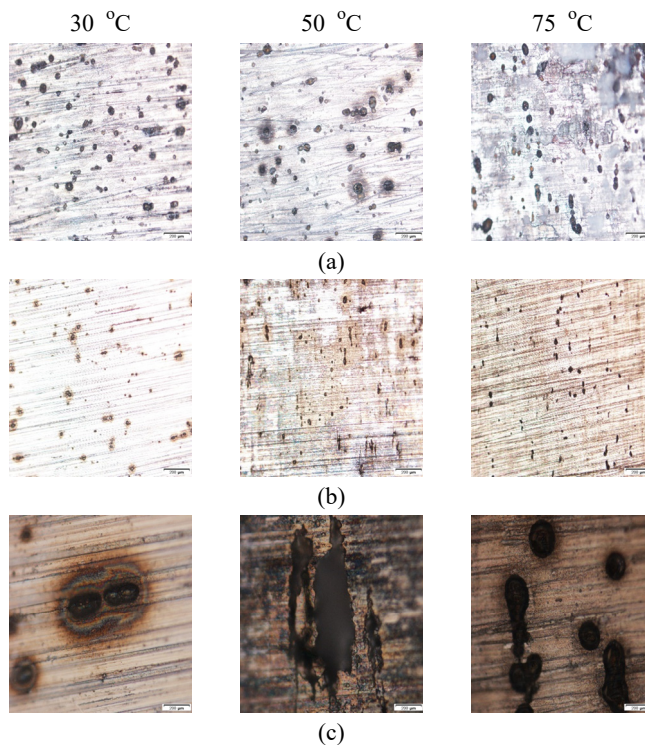
Fig. 7 Effect of solution temperature in 0.1% NaCl on the surface appearance of AA7075T6 after the corrosion tests in 0.1% NaCl solution; (a) single specimen (OM, x100) and (b) galvanic coupled specimen with CFRP (OM, x100) (c) galvanic coupled specimen with CFRP (OM, x1000).
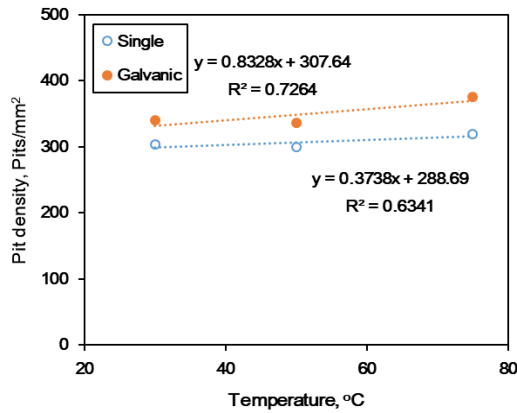
Fig. 8 Relationship between solution temperature and pit density of AA7075T6 by galvanic coupling with CFRP (NaCl concentration; 0.1%).
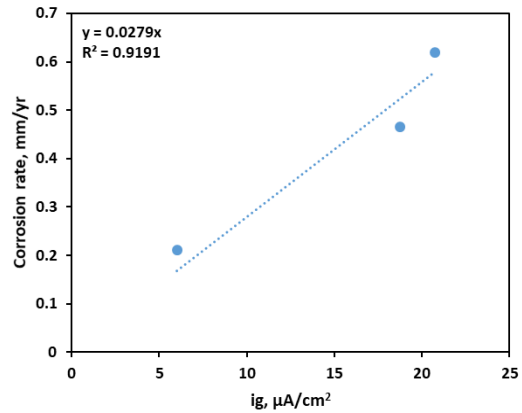
Fig.10 Effect of solution temperature on the relationship between galvanic current density derived from the mixed potential theory using polarization curves and the corrosion rate of AA7075T6 by galvanic coupled CFRP.
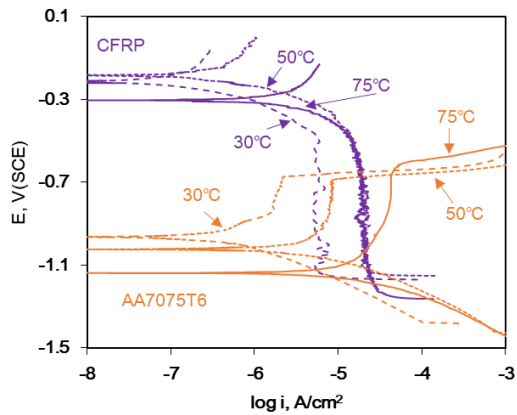
Fig. 9 Combination between cathodic polarization curve of CFRP and anodic polarization curve of AA7075T6 in deaerated 0.1% NaCl solution at (30, 50, and 75) $^{\circ}$C.

the mixed potential theory using polarization curves and the corrosion rate of AA7075T6 by galvanic coupled CFRP. Two factors show the exponential relation:

Corrosion rate, mm/yr = 0.0279 x [i_g, μA/cm^2].

4. Conclusions

This work focused on the effect of NaCl concentration of (0.01, 0.1, and 1)% NaCl and solution temperature of (30, 50, and 75) $^{\circ}$C on the corrosion between CFRP and AA7075 aluminum alloy. The following can be concluded.

1) On increasing the NaCl concentration or solution temperature, the galvanic corrosion rate of AA7075T6 by CFRP was increased several hundred times over that of the single specimens, and the effects of NaCl concentration or solution temperature on the increasing of the corrosion rate in the galvanic coupled specimen were higher than that in the single specimen.

2) Regardless of the specimen being single or galvanic coupled, the relationships between NaCl concentration and pit density were logarithmic trends, but the relationships between solution temperature and pit density were linear trends.

by galvanic coupling with CFRP. The NaCl concentration was 0.1%. As the solution temperature, and pit density slightly increased, the relationship between solution temperature and pit density revealed a linear trend.

Fig. 9 reveals the combination between the cathodic polarization curve of CFRP and the anodic polarization curve of AA7075T6 in deaerated 0.1% NaCl solution. Regardless of the solution temperature, the cathodic polarization curves of CFRP meet the anodic polarization curves above the pitting potentials except at 75 $^{\circ}$C. This means that galvanic coupling with CFRP can facilitate the corrosion of AA7075T6.

The galvanic corrosion current density can be calculated from Fig. 9 based on the mixed potential theory. Fig. 10 shows the effect of solution temperature on the relationship between galvanic current density (i_g) derived from

References

1. A. A. Younis, M. M. B. El-sabbah, and R. Holz, *J.*

Solid State Electrochem., **16**, 1033 (2012). https://doi.org/10.1007/s10008-011-1476-7

2. B. Zaid, D. Saidi, A. Benzaid, and S. Hadji, *Corros. Sci.*, **50**, 1841 (2008). https://doi.org/10.1016/j.corsci.2008.03.006

3. Y. Wang, G. Cheng, W. Wu, Q. Qiao, Y. Li, and X. Li, *Appl. Surf. Sci.*, **349**, 746 (2015). https://doi.org/10.1016/j.apsusc.2015.05.053

4. Z. S. Smialowska, *Corros. Sci.*, **41**, 1743 (1999). https://doi.org/10.1016/S0010-938X(99)00012-8

5. I. W. Huang, B. L. Hurley, F. Yang, and R. G. Buchheit, *Electrochim. Acta*, **199**, 242, (2016). https://doi.org/10.1016/j.electacta.2016.03.125

6. H. Ezuber, A. E. Houd, and F. E. Shawesh, *Mater. Design*, **29**, 801 (2008). https://doi.org/10.1016/j.matdes.2007.01.021

7. G. S. Frankel, *J. Electrochem. Soc.*, **145**, 2186 (1998). https://doi.org/10.1149/1.1838615

8. Y. R. Yoo, Y. I. Son, G. T. Shim, Y. H. Kwon, and Y. S. Kim, *Corros. Sci. Tech.*, **8**, 27 (2009). http:/www.j-cst.org/main/abstract_view.htm?scode=C &code=C00080100027&vol=8&no=1&type=aissue

9. Y. S. Kim, H. K. Lim, Y. I. Sohn, Y. R. Yoo, and H. Y. Chang, *Corros. Sci. Tech.,* **9**, 39(2010). http://www.j-cst.org/main/abstract_view.htm?scode=C &code=C00090100039&vol=9&no=1&type=aissue

10. Y. R. Yoo, Y. I. Son, G. T. Shim, Y. H. Kwon, and Y. S. Kim, *Korean J. Met. Mater.*, **48**, 514 (2010).

11. Z. Peng and X. Nie, *Surf. Coat. Technol.*, **215**, 85 (2013). https://doi.org/10.1016/j.surfcoat.2012.08.098

12. H. Jiang, Y. Cong, X. Zhang, G. Li, and J. Cui, *Mater. Design*, **142**, 297 (2018). https://doi.org/10.1016/j.matdes.2018.01.047

13. E. Hakansson, J. Hoffman, P. Predecki, and M. Kumosa, *Corros. Sci.*, **114**, 10 (2017). https://doi.org/10.1016/j.corsci.2016.10.011

14. M. Mandel and L. Kruger, *Mater. Sci. Eng. Technology (Materialwiss. Werkstofftech.)*, **4**, 43 (2012). https://doi.org/10.1002/mawe.201200945

15. S. Palani, T. Hack, J. Deconinck, and H. Lohner, *Corros. Sci.*, **78**, 89 (2014). https://doi.org/10.1016/j.corsci.2013.09.003

16. Z. Liu, M. Curioni, P. Jamshidi, A. Walker, P. Prengnell, G. E. Thompson, and P. Skeldon, *Appl. Surf. Sci.*, **314**, 233 (2014). https://doi.org/10.1016/j.apsusc.2014.06.072

17. S. Y. Hur, K. T. Kim, and Y. S. Kim, *Corros. Sci. Tech.*, **18**, 129 (2019). http://www.j-cst.org/main/abstract_view.htm?scode=C &code=C00180400129&vol=18&no=4&type=aissue

18. ASTM B221, Standard specification for aluminum and aluminum-alloy extruded bars, rods, wire, profiles, and tubes, ASTM (2012).

19. M. G. Fontana, *Corrosion Engineering*, *3rd ed.*, p. 462, McGraw-Hill, Singapore (1987).